Inorganic Chemistry
Cite This: Inorg. Chem. XXXX, XXX, XXX−XXX
Article
pubs.acs.org/IC

o-Carborane, Ferrocene, and Phthalocyanine Triad for High-Mobility Organic Field-Effect Transistors

Ilgın Nar,[†] Armağan Atsay,[†] Ahmet Altındal,[‡] and Esin Hamuryudan*,[†]

[†]Faculty of Science and Letters, Department of Chemistry, İstanbul Technical University, 34469 Maslak, Istanbul, Turkey
[‡]Faculty of Science and Art, Department of Physics, Yıldız Technical University, 34722 Esenler, Istanbul, Turkey

Supporting Information

ABSTRACT: An unsymmetrical zinc phthalocyanine with ferrocenylcarborane linked to the phthalocyanine ring through a phenylethynyl spacer was designed for organic field-effect transistor (OFET). The unsymmetrical phthalocyanine derivatives were characterized using a wide range of spectroscopic and electrochemical methods. In particular, the ferrocenylcarborane structure was unambiguously revealed based on the single-crystal X-ray diffraction analysis. In-depth investigations of the electrochemical properties demonstrated that the ferrocenylcarborane insertion extended the electrochemical character of ferrocenylcarborane-substituted phthalocyanine (**7**). Moreover, in the anodic potential scans, the oxidative electropolymerization of etynylphthalocyanine (**6**) and **7** was recorded. To clarify the effect of the insertion of ferrocenylcarborane (**2**) on the field-effect mobility, solution-processed films of **2**, **6**, and **7** were used as an active layer to fabricate the bottom-gate top-contact OFET devices. An analysis of the output and transfer characteristics of the fabricated devices indicated that the phthalocyanine derivative functionalized with ferrocenylcarborane moiety has great potential in the production of high-mobility OFET.

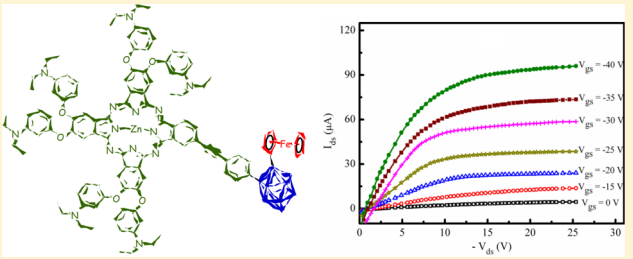

INTRODUCTION

Because of the growing need in advanced technological applications, multifunctional organic materials have received increasing attention.[1] Organic semiconducting materials are an essential component of organic electronic devices, and considerable effort has been expended to develop organic field-effect transistor (OFET) materials.[2] Although important advances have been made toward high-performance OFET device, a lot of improvement remains necessary for practical applications. The poor charge carrier mobility is the main drawback of organic semiconductors for use as active layers in OFETs.[3] Therefore, the synthesis of a suitable organic active layer with high capacitance and field-effect mobility is essential to achieve the desired OFET performance. Recent studies show that the charge carrier mobility can be improved when an electron-donating or -withdrawing group is combined with the aromatic system, which enables the formation of functional devices.[2g,4]

Phthalocyanines are some of the most important π-conjugated molecules in electronics and optoelectronics.[5] Associated with their large conjugated molecular structure, phthalocyanine (Pc)-based systems have interesting properties such as high thermal, photo, and chemical stabilities.[6] These attributes make them excellent precursors for functional materials, which may be applied in photovoltaic cells and OFETs.[7] Improvements in solubility and control of the molecular arrangement of phthalocyanines are important properties for the development of OFETs. The key point of OFET development for phthalocyanine compounds is to design and prepare materials with excellent solubility and high stability.[7b−d,8]

Meanwhile, *o*-carborane is a polyhedral electron-deficient boron cluster that contains two adjacent carbon atoms with a three-dimensional delocalization of the electrons, which has a highly polarizable σ-aromatic character, so they can electronically interact with π-conjugated systems.[9] The cluster has electron-withdrawing character when it is bonded through carbon vertices.[10] In addition, methyl groups on boron are electron-withdrawing when carboranes are partially methylated.[11] Because of their thermal stability, the incorporation of these systems into different structures results in improved thermally and chemically stable materials. The recent use of carborane clusters in material science has focused on the development of nonlinear optics,[12] boron-rich dendrimers,[13] photovoltaic devices,[14] ion transporters,[15] quantum dots,[16] and luminescent materials.[17] Carborane-containing OFETs have recently been reported.[18] An excellent electron-transport compound buckminsterfullerene and electron-withdrawing *o*-carborane-including compounds have been studied for OFET applications. A shorter distance between carborane and C_{60} corresponds to higher electron mobility of the FET.[18]

Despite numerous studies on the synthesis and OFET properties of phthalocyanines and carboranes, to the best of our knowledge, no prior publication has documented a compound that includes these two units. Here, we report the synthesis,

Received: December 8, 2017

DOI: 10.1021/acs.inorgchem.7b03097
Inorg. Chem. XXXX, XXX, XXX−XXX

Scheme 1. Synthetic Route to 1 and 2

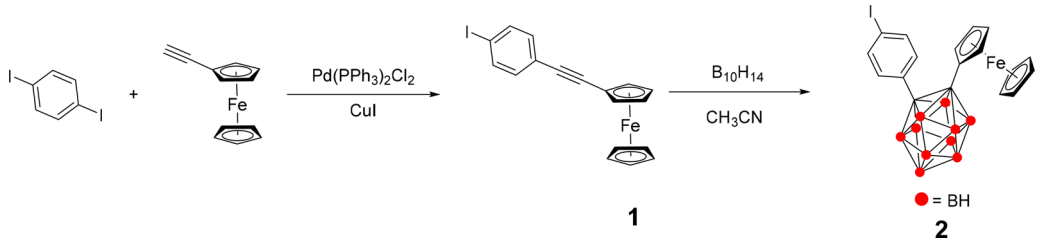

Scheme 2. Synthetic Route to 5, 6, and 7

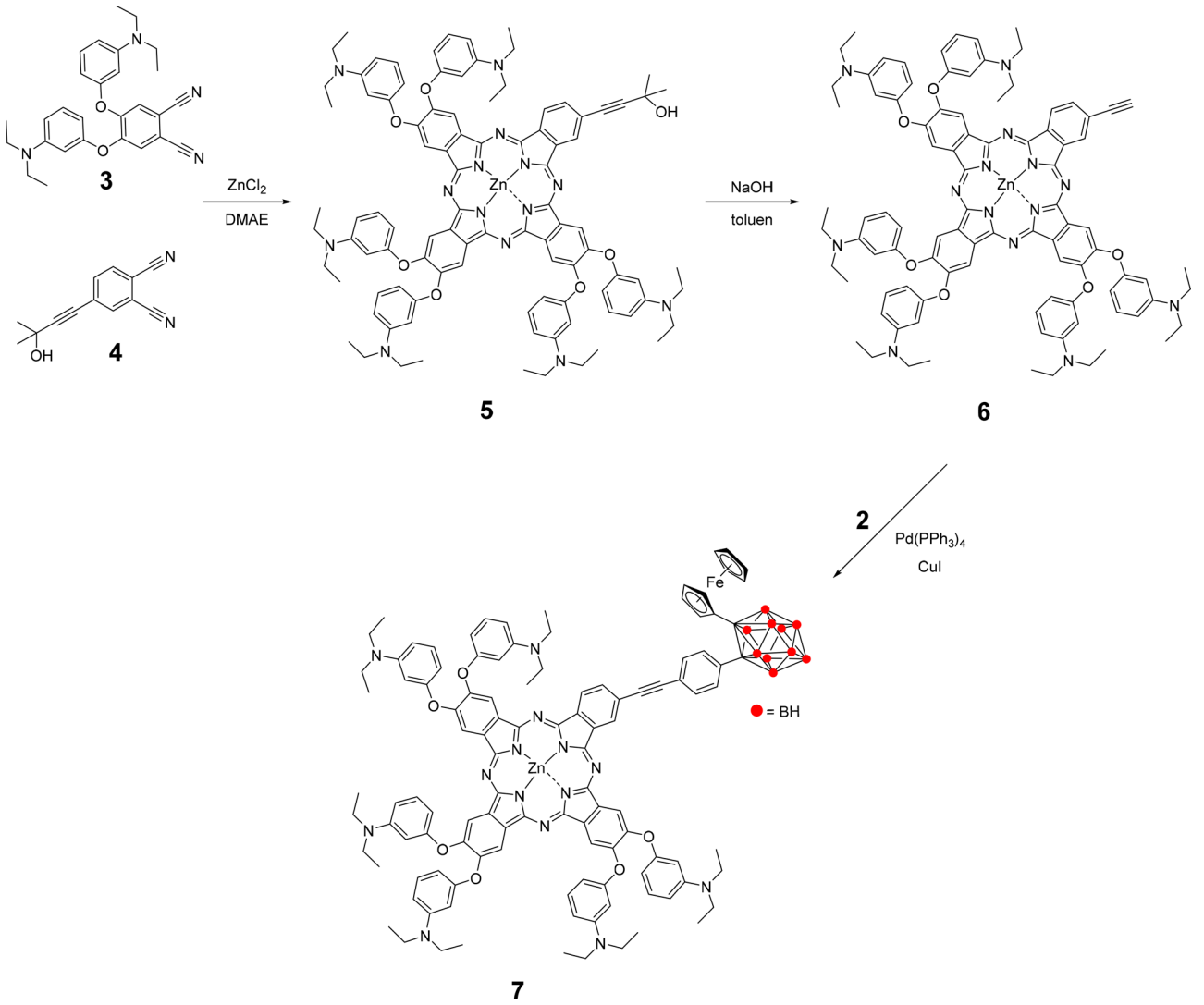

characterization, and OFET properties of a new phthalocyanine-carborane-ferrocene triad system.

RESULTS AND DISCUSSION

The interest of phthalocyanine-based materials lies in their versatility as molecular building blocks, and their properties can be tuned using different peripheral substituents. Among various introduced substituents, carborane-substituted phthalocyanines are rare. In this paper, we synthesize a new phthalocyanine−carborane conjugate, which consists of an unsymmetrical substituted zinc phthalocyanine linked to a ferrocenylcarborane subunit by an arylene−alkynylene spacer, and their potential as an active layer in OFETs were investigated.

Ferrocenylcarborane was prepared in two steps (Scheme 1). Sonogashira cross-coupling reaction of ethynyl ferrocene with 1,4-diiodobenzene in triethylamine (TEA)/toluene mixture in the presence of $Pd(PPh_3)_2Cl_2$ as a catalyst and CuI as a cocatalyst resulted in 4-iodo-1-ferrocenyl-ethynylbenzene (**1**).[19] The reaction of the intermediate **1** with decaborane in the presence of acetonitrile and toluene produced the *o*-carborane compound (**2**) in moderate yield (38%).

The introduction of bulky substituents onto the phthalocyanine ring is a common method to reduce aggregation and increase the solubility.[20] In this manner, 4,5-bis(3-

DOI: 10.1021/acs.inorgchem.7b03097
Inorg. Chem. XXXX, XXX, XXX−XXX

diethyaminophenoxy)phthalonitrile (**3**) as a precursor for the phthalocyanine synthesis was synthesized according to a well-known method from 4,5-dichlorophthalonitrile and 3-diethylaminophenol.[21] The other phthalonitrile derivative 4-(3-hydroxy-3-methyl-1-butynyl)phthalonitrile (**4**) was prepared as described in the literature.[22]

6 was prepared in two steps. The mixed condensation of 4-(3-hydroxy-3-methyl-1-butynyl)phthalonitrile with 4,5-bis(3-dietylaminophenoxy) phthalonitrile in the presence of zinc chloride afforded the unsymmetrical **5** in 20.2% yield (Scheme 2). Then, the $-C(CH_3)_2OH$ protecting group of the ethynyl function in **5** was removed as acetone by a treatment with sodium hydroxide in toluene to produce the terminal alkyne **6** in 72% yields.[23]

7 was prepared in 62% yield from the Pd-catalyzed Sonogashira coupling between unsymmetrically ethynyl-substituted **6** and **2**.

Because multiple bulky lipophilic groups were attached at the periphery, **7** was notably soluble in common organic solvents. Satisfactory elemental analysis results were obtained for the newly prepared phthalocyaninato zinc derivatives after repeated column chromatography. These newly prepared phthalocyanine derivatives were also characterized using other spectroscopic methods including one-dimensional (1D) and two-dimensional (2D) NMR, Fourier transform infrared (FT-IR), mass spectrometry (MS), and electronic absorption spectroscopy. The detailed characterization of compounds can be found in the Supporting Information.

In addition, compound **2** was characterized by a single-crystal X-ray diffraction analysis (Table S1). The molecular structure of compound **2** is shown in Figure 1 with the indicated atom-

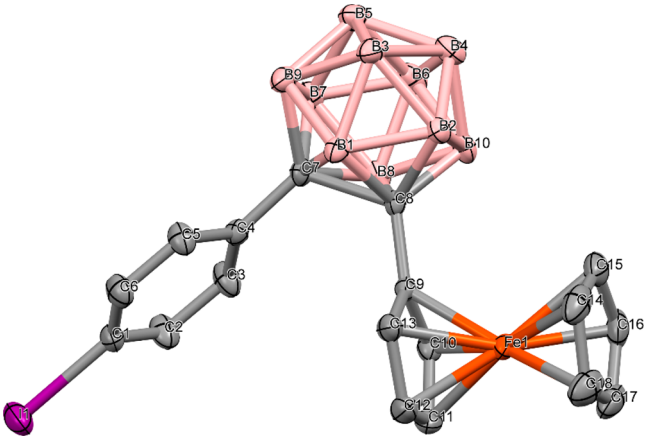

Figure 1. X-ray structure of **2**, which shows the atom labeling and displacement ellipsoids at the 30% probability level. (*Hydrogen atoms are omitted for clarity*).

numbering schemes. Single crystals of **2** were obtained by slowly evaporating a saturated chloroform/methanol solution at room temperature. **2** crystallizes in the orthorhombic *Pbca* space group. The observed mean bond lengths of compound **2** Fe−C of the ferrocene moiety and B−C and B−B of the *o*-carborane cage (Fe−C 2.043 Å, B−C 1.72 Å, B−B 1.773 Å) are consistent with the reported values.[24] The C−C bond length of 1,2 disubstituted *o*-carboranes shows large variations depending on electronic and steric effects of substituents; in **2** the observed C−C bond length of *o*-carborane cage is 1.74 Å.[25] The dihedral angle between the cyclopentadienyl ring and the C−C bond of *o*-carborane at the C(9) position of the cyclopentadienyl ring plane is approximately in an orthogonal position with 91.16° for C(7)−C(8)−C(9)−C(10). The torsional angle of C(3)−C(4)−C(7)−C(8), which depicts the phenyl group conformation with respect to the C−C bond of *o*-Carborane, is 82.97°.

In the FT-IR spectra of **6**, the disappearance of O−H bands at 3296 cm^{-1} and formation of the −CC-H group absorption at 3279 cm^{-1} clearly indicate the deprotection of the protecting group as acetone. The disappearance of the −CC-H band and formation of the B−H stretching vibrations at 2575 cm^{-1} indicate the conversion of Pc **6** to **7**.

As shown in Figure 2, the complexes **5**, **6**, and **7** have similar ^{1}H NMR spectra. The disappearance of the peak at 1.8 ppm indicates the conversion of **5** to **6**. After the conversion of **6** to **7**, in the ^{1}H NMR spectrum of **7**, it is possible to assign the signals corresponding to the ferrocene subunit, that is, two triplets centered at δ = 4.04 and 4.23 ppm for the substituted cyclopentadienyl ring and a broad singlet at δ = 4.22 ppm for the unsubstituted one.[26] The proton chemical shifts of the phenyl spacer bonded to the carborane unit are assigned at 7.41−7.45 ppm as a multiplet. In the ^{1}H NMR spectrum of **7**, the B−H proton chemical shifts of carborane unit are not clearly observed because of the coupling to quadrupole ^{11}B nuclei. When a proton spectrum is acquired with ^{11}B decoupling, multiple broad signals of the B−H proton chemicals shifts are observed at 3.1−2 ppm[27] (Figure 2). The ^{13}C NMR spectra of compound **5**, **6**, and **7** are consistent with the structures. In the ^{13}C NMR spectrum of **7**, we can assign the signals to the ferrocene subunit, that is, the signals at 71.22, 68.79, and 82.88 ppm for the substituted cyclopentadienyl ring and that at 70.40 ppm for the unsubstituted one. The ^{13}C chemical shifts of *o*-carborane unit are observed at 84.98 and 85.50 ppm.

The ^{11}B NMR chemical shift of compound **2** was observed at −2.34, −3.39, −8.94, −9.26, −10.46, and −11.37 ppm, and the ^{11}B chemical shift of **7** had two broad signals at −2.05 and −9.89 ppm.

The electronic absorption spectra of **5**, **6**, and **7** were recorded in CH_2Cl_2. Their spectra show a typical phthalocyanine Soret band at ∼355 nm with medium intensity and a notably strong Q-band at ∼685 nm with a weak vibronic shoulder at 620 nm.[28]

The phthalocyanines exhibit molecular-ion peaks at m/z = 1636.446 $[M]^+$ for **5**, 1578.659 $[M]^+$ for **6**, and 1982.192 [M]+ for **7** in their mass spectra without significant fragmentation.

ELECTROCHEMICAL PROPERTIES

The redox properties of **2**, **6**, and **7** were characterized using cyclic voltammetry (CV). The measurements were performed in anhydrous dichloromethane (DCM) using tetra-*n*-butylammonium perchlorate (TBAP) as the supporting electrolyte. The electrochemical data are listed in Table 1, and the representative cyclic voltammograms of **2**, **6**, and **7** are shown in Figure 3.

Ferrocenylcarborane (**2**) gives two reversible electrochemical reactions at $E_{1/2}$ = −1.28 V and $E_{1/2}$ = 0.88 V, which are attributed to carborane and ferrocene, respectively.[24] Phthalocyanine **6** shows two phthalocyanine ring-based reversible one-electron reduction couplings at $E_{1/2}$ = −0.78 V and −1.10 V and two ring-based oxidations at 0.85 and 0.96 V. Although the zinc metal ion cannot oxidize or reduce in this electrochemical

DOI: 10.1021/acs.inorgchem.7b03097
Inorg. Chem. XXXX, XXX, XXX−XXX

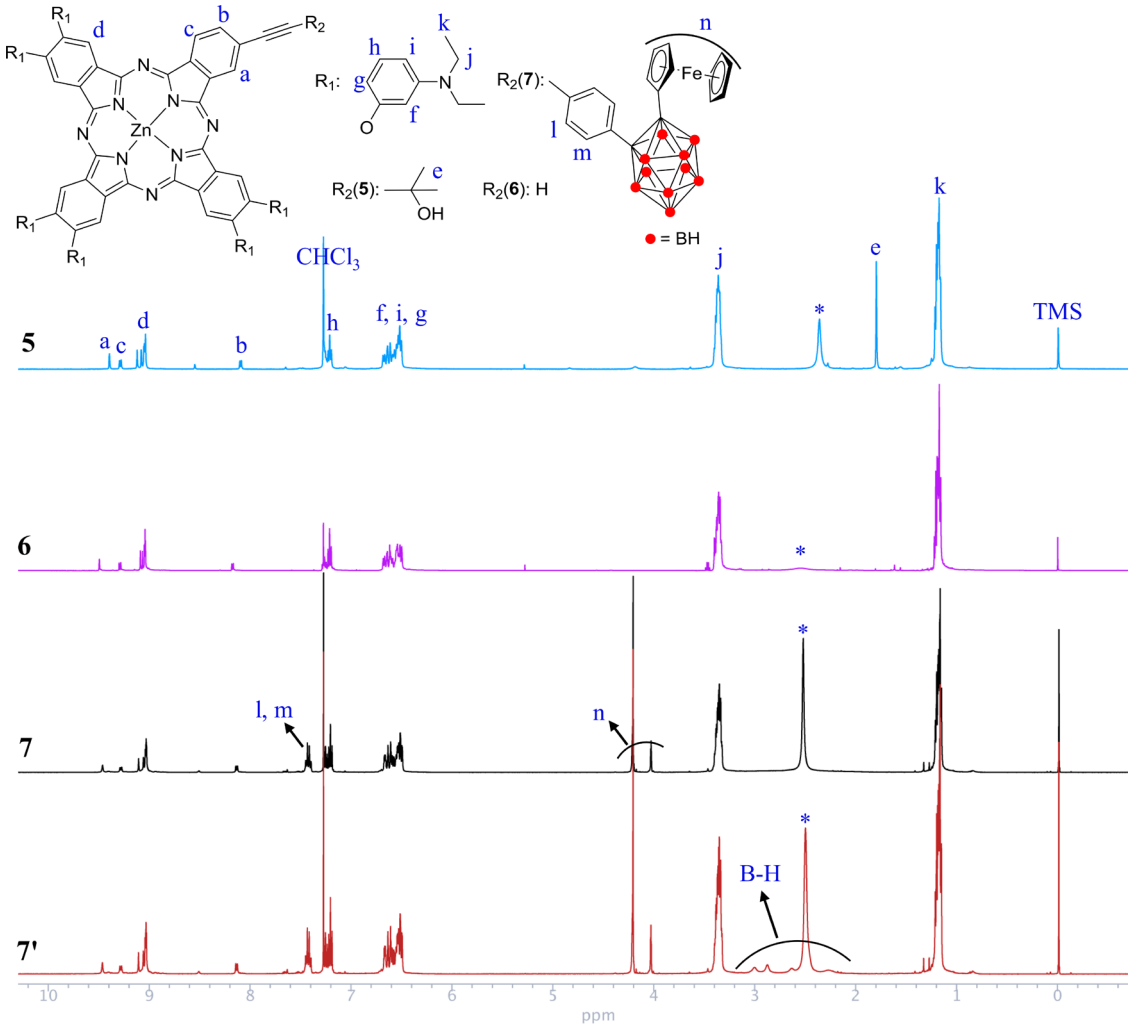

Figure 2. ^{1}H NMR spectrum of **5**, **6**, **7**, and **7′** (^{11}B decoupled ^{1}H). Residual water denoted as *.

Table 1. Electrochemical Properties[a] of the Compounds 2, 6, and 7

compound	E^{2}_{red}	E^{1}_{red}	E^{1}_{oxid}	E^{2}_{oxid}
2		−1.28	0.88	
6	−1.10	−0.78	0.85	0.96
7	−1.26	−0.84	0.84	0.98

[a]Ferrocene gives a redox couple at 0.60 V versus SCE.

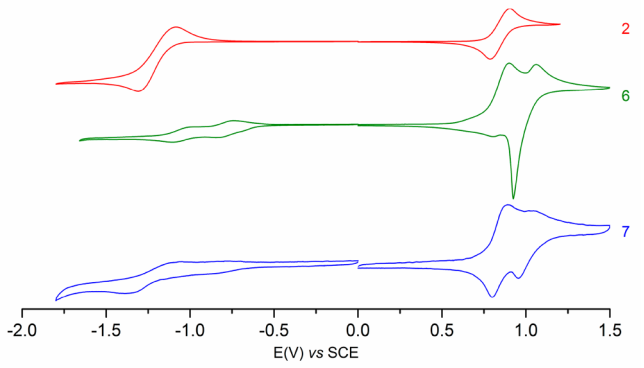

Figure 3. Cyclic voltammograms of **2**, **6**, and **7** in CH_2Cl_2 with 0.1 M TBAP at a scan rate of 25 mV s^{-1}.

range, all processes are attributed to the removal/addition of one electron from/to the ligand-based orbitals of phthalocyanine.[29] **7** has cathodic-shifted two-ring reduction processes, and the second reduction potential could not be exactly determined because of the overlapping of the one-electron phthalocyanine reduction and carborane unit. Reduction potentials of **7** shifts to negative regions compared to **6** because of the electron-withdrawing character of carborane. In anodic scans, two oxidation processes were observed. Because of overlapping of the one-electron phthalocyanine oxidation and ferrocene unit the first oxidation potential could not be exactly determined. In addition, in the anodic potential scans, oxidative electropolymerization of **6** and **7** was recorded (see Figure S30).[21b,30] Overall, addition of ferrocenylcarborane moiety to **6** enhanced reversible electrochemical processes.

OFET STUDIES

The dielectric performance of the passivation layer, which is poly(vinyl alcohol) (PVA) in our case, must be investigated to extract the main performance parameters from the measured transfer and output characteristics of an OFET device. Therefore, we first examine the insulating properties of the PVA film, which will be used as the gate dielectric. One of the most important performance indicators for an insulator layer is the capacitance density. A high capacitance density is desirable

DOI: 10.1021/acs.inorgchem.7b03097
Inorg. Chem. XXXX, XXX, XXX−XXX

in OFET applications. The frequency-dependent capacitance measurement is a widely used technique to characterize the capacitive behavior of an insulator. Therefore, the dielectric behavior of the PVA film was evaluated by producing a parallel-plate capacitor with the structure of indium tin oxide (ITO)/PVA/Au. For this purpose, the capacitance measurements were performed using an impedance analyzer (HP 4192A) in a frequency range of 5 Hz−2 MHz under ambient conditions (relative humidity (RH) ≈ 45%; 27 °C), and the results are shown in Figure 4. Figure 4 shows a strong frequency

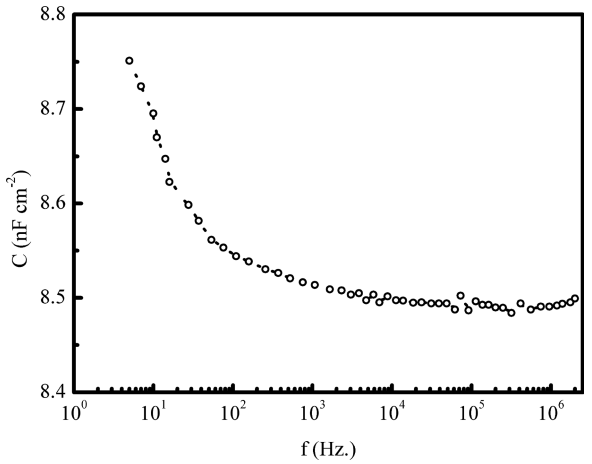

Figure 4. Frequency dependence of the capacitance density in the ITO/PVA/Au structure.

dispersion at low frequencies and a nearly frequency-independent behavior in the high-frequency region. A capacitance density of 8.75 nF/cm^2 was obtained at a frequency of 5 Hz with slightly smaller values at higher frequencies (Figure 4).

In a p-channel OFET, when a positive voltage is applied to the gate electrode with respect to the source electrode, a depletion region forms, which corresponds to the high-channel-resistance state. The charge carriers in the channel region accumulate when the gate voltage is reversed, which corresponds to a low-channel-resistance state. To compare the performance of compounds **2**, **6**, and **7** as the active layer in OFETs, the output and transfer characteristics of the devices were analyzed. The variation of the drain-source current (I_{ds}) with the drain-source voltage (V_{ds}) (output characteristic) for various gate-source voltages (V_{gs}) between 0 and −40 V is shown in Figure 5a−c for all investigated devices. The analysis of the output characteristics of the devices shows that the drain-source current for the **7**-based device is 47 and 235 times higher than those of the **2** and **6** based devices, respectively. Note that the current I_{ds} increases with the increase in negative V_{GS} voltage for all devices (Figure 5a−c). The dependence of current I_{ds} on negative V_{gs} voltage indicates the p-type behavior of the active layers (when a negative bias voltage is applied to the gate electrodes, holes accumulate in the channel region).

At low V_{ds} voltages, I_{ds} linearly increases with the applied V_{ds} voltage, which indicates that the lower voltage region can be considered ohmic. In this region, the relation between I_{ds} and V_{ds} is as follows.[31]

$$I_{ds} = \frac{W}{L} C_i \mu_p (V_{ds} - V_{th}) V_{ds} - \frac{1}{2} {V_{ds}}^2 \quad (1)$$

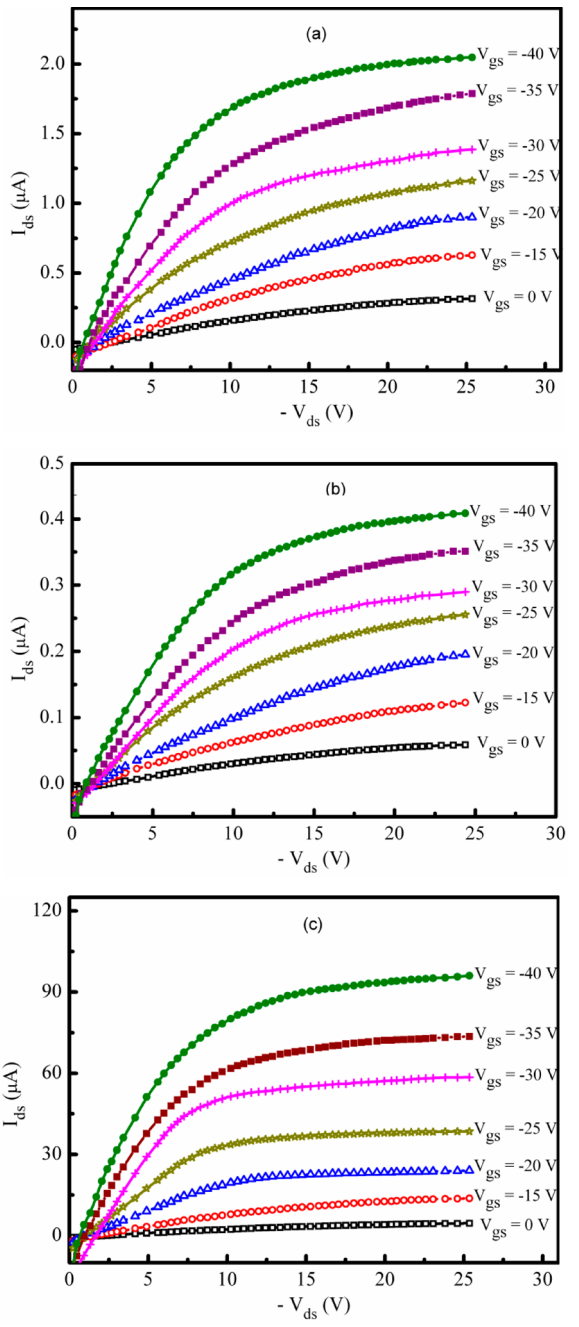

Figure 5. Output characteristics of the **2**-, **6**-, and **7**-based OFETs with PVA as the gate dielectric.

where W and L are the channel width and length, respectively; μ_p is the field effect mobility for p-type charge carriers; C_i is the insulator capacitance per unit area; V_{th} is the threshold voltage. For low values of the applied V_{ds} voltage, the ${V_{ds}}^2$ term on the right-hand side of eq 1 is negligible. Then, the dependence of current I_{ds} on voltage V_{ds} can be expressed as

$$I_{ds} = \frac{W}{L} C_i \mu_p (V_{ds} - V_{th}) V_{ds} \quad (2)$$

Figure 5 shows that the increase in current I_{ds} with voltage V_{ds} does not continue as a straight line with further increase in V_{ds}; a saturation tendency of I_{ds} is clear when V_{ds} was increased. In this V_{ds} voltage region, the dependence of I_{ds} on V_{gs} is more significant than that of V_{ds}. A reasonable explanation for the

DOI: 10.1021/acs.inorgchem.7b03097
Inorg. Chem. XXXX, XXX, XXX−XXX

strong V_{gs} dependency of current I_{ds} at higher values of V_{ds} is as follows: when voltage V_{ds} increases, the voltage difference between the source terminal of the OFET and the points along the channel region decreases. In this case, the width of the channel region is no longer uniform, and its resistance correspondingly increases, which is known as the pinch-off of the channel. The observed saturation tendency of I_{ds} can be attributed to the pinch-off of the channel.

For the saturation region, the relation between I_{DS} and V_{GS} is[32]

$$I_{DS} = \frac{W}{2L} C_i \mu_p (V_{gs} - V_{th})^2 \quad (3)$$

The analysis of the experimentally obtained output characteristics shows that the **7**-based device exhibits better performance than the **2**- and **6**-based devices. An I_{ds} current of 9.6×10^{-5} A at a gate-source voltage of −40 V was observed for the **7**-based OFET device, whereas the maximum value of I_{ds} for the **2**- and **6**-based devices was 2.0×10^{-6} A and 4.1×10^{-7} A, respectively. The improvement in I_{ds} for the **7**-based OFET device is attributed to the presence of the carborane conjugate, which was linked to a ferrocenylcarborane subunit via an arylene−alkynylene spacer.

The field-effect mobility and threshold voltage are considered important parameters that characterize an OFET. These parameters can be obtained using various methods. In this work, the mobility values of all devices were extracted from a plot of the square root of I_{ds} versus V_{gs} by fitting data to eq 3. The recorded transfer characteristic of the investigated devices is shown in Figure 6 on a log scale as a function of V_{gs} for a

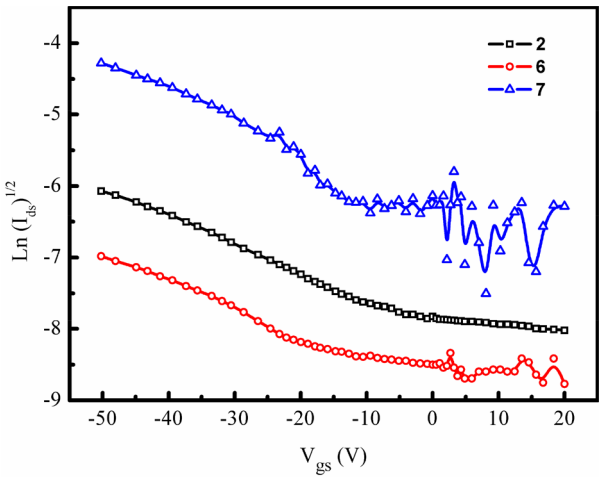

Figure 6. Transfer characteristics of the **2**-, **6**-, and **7**-based OFET device.

constant V_{ds} of −20 V. From the slopes of the transfer characteristic of the devices, using eq 3, the field-effect mobility was determined.

The **7**-based device has a field effect mobility of 4.7×10^{-1} cm^2/V s, which was 6 and 17 times larger than those of the **2**- and **6**-based devices. The obtained mobility values for the **2**- and **6**-based OFET are 6.9×10^{-2} and 2.7×10^{-2} cm^2/V s, respectively. The observed field effect mobility, particularly in compound **7**, was higher than those of similar devices in the literature.[7a,33] For efficient charge-carrier injection, a good matching of the energy level between the organic semiconductor and the electrode and a large π-orbit overlap are necessary. It is also well-established that the molecular orientation of the Pc molecules in the solid state is of great interest, because it is believed to strongly affect the carrier mobility in electronic devices. As mentioned above, on the one hand, it is well-documented in literature that the charge-carrier mobility in OFETs critically on the nanomorphology of the active layer, molecular ordering degree, and $\pi-\pi$ stacking extent. On the other hand, numerous studies in recent years have shown that the incorporation of carborane unit into organic π-systems stabilizes the lowest unoccupied molecular orbital level by direct contribution to orbital delocalization, as well as by inductive electron-withdrawing effect. A detailed literature survey indicates that the introduction of novel electron accepting auxiliary, such as *o*-carborane, into the π-system of organic molecules improves their electron transfer ability and can be utilized as electron transfer mediator in electrocatalytic reductions. Therefore, it can be concluded that the incorporation of *o*-carborane as an electron-accepting and/or transporting auxiliary into Pcs affects the electron transporting properties of Pcs, thereby modulating the charge carrier mobility in phthalocyanine-based OFET devices.[18a,34] An overall evaluation of the experimental data reveals that the ferrocenylcarborane subunit has a strong effect on the charge carrier mobility in OFET applications.

EXPERIMENTAL SECTION

Materials, Instruments, and Methods. All NMR spectra were recorded on Agilent VNMRS 500 MHz at 25 °C, and chemical shifts were referenced internally using the residual solvent resonances. Matrix-assisted laser desorption time-of-flight mass spectrometry (MALDI-TOF-MS) was performed on Bruker Daltonics Ultraflex MALDI TOF mass spectrometer. IR spectra were recorded on a PerkinElmer Spectrum One FT-IR (ATR sampling accessory) spectrophotometer; electronic spectra were recorded on a Scinco S-3100 spectrophotometer. The elemental analysis was performed on a Costech ECS 4010 CHNS elemental analyzer. All reagents and solvents were of reagent-grade quality obtained from commercial suppliers. Electrochemical measurements were performed using a Gamry 600 potentiostat/galvanostat. Electrochemical behaviors were performed by CV with a glassy carbon working, a platinum wire counter, and a saturated calomel (SCE) reference electrode. Typically, a 0.1 M solution of TBAP in CH_2Cl_2 containing the sample was purged with nitrogen for 20 min, and then the voltammograms were recorded at room temperature at 25 mV scan rate. **1**,[19] **3**,[21b] and **4**[21a,22] were synthesized according to literature procedures.

Single crystal of **2** was obtained by slow evaporation of saturated chloroform/methanol solution of **2** at room temperature. Single crystal of **2** was mounted on a MicroMount (MiTeGen). Crystallographic data of the compounds were recorded on a Bruker D8 VENTURE single-crystal X-ray diffractometer equipped with PHOTON 100 CMOS detector at 292 K, using graphite monochromatized Mo Kα radiation (λ = 0.710 73 Å). All of the data were corrected for absorption effects using the multiscan technique. The structures were solved by direct methods and refined on F^2 by full matrix least-squares using SHELXL 2014.[35] All the hydrogen atoms were added to their geometrically ideal positions. All non-hydrogen atoms were refined with anisotropic displacement parameters. The crystal and instrumental parameters used in the unit-cell determination and data collection are summarized in Table S1. Crystallographic figures were drawn using Mercury software.[36]

Fabrication of OFET Devices and Their Characterization. Bottom-gate top-contact OFET devices were fabricated on ITO-coated glass substrates. Commercially available PVA (Mw = 80 000 to 120 000) was used as gate insulator for all OFET devices investigated. After the cleaning of the ITO substrate by ultrasonic treatment in isopropyl alcohol, acetone, and deionized water, respectively, the gate dielectric was deposited from a solution of 40 mg/mL PVA in

DOI: 10.1021/acs.inorgchem.7b03097
Inorg. Chem. XXXX, XXX, XXX−XXX

deionized water by spin-coating procesess at 1200 rpm during 90 s. After the depositon of gate dielectric, the samples were dried at 140 °C for 120 min, following a procedure described by Sun et al.[37] Then, on the top of the gate dielectrics, a solution of Pc compound **2**, **6**, and **7** in DCM with a concentration of 3×10^{-3} M as active layer was spun. The thickness of the active layer was fixed at 180 nm. The thickness of the Pc films was measured by elipsometric technique. The error in the measurement of the thickness of the Pc films is estimated at ∼1%. After the deposition of active layer, to remove the remaining solvent in the film, films of the Pc compound were dried in a vacuum oven at 130 °C for 30 min. The substrate was immediately placed in a vacuum system for the deposition of source-drain contacts after the deposition of the active layer. Gold source-drain electrodes (400 nm) were then deposited onto the active layer through a shadow mask with a channel length (L) of 80 μm and a width (W) of 4 mm. The transfer and output characteristics of the fabricated devices were measured in atmospheric conditions using a Keithley 617 programmable electrometer and a Keithley 2400 source-meter.

Synthesis. *1-p-Iodophenyl-2-ferrocenyl-o-carborane (**2**).* Decaborane (500 mg, 4.10 mmol) was dissolved in 20 mL of acetonitrile and toluene mixture (1:1) under nitrogen atmosphere. The mixture was stirred under reflux for 2 h. After this cooled to room temperature, **1** (2.05 mmol) was added, and the mixture was additionally refluxed for 2 d. After this cooled to room temperature, insoluble products were removed by filtration, and the solvent was evaporated. The residue was purified by column chromatography on a silica gel using hexane as eluent.

Yield: 420 mg (38%); **^{1}H NMR** (500 MHz, CDCl$_3$, 25 °C), δ 7.47−7.45 (d, 2H), 7.09−7.07 (d, 2H), 4.21 (s, 5H), 4.18 (t, 2H), 4.02 (t, 2H), 3.51−1.82 (b, 10H) ppm. **^{13}C NMR** (126 MHz, CDCl$_3$, 25 °C), δ 137.17, 132.33, 130.78, 96.89, 85.19, 84.36, 82.78, 71.15, 70.50, 68.79 ppm. **^{11}B NMR** (CDCl$_3$, 25 °C), δ −2.34, −3.39, −8.94, −9.26, −10.46, −11.37 ppm.

*2,3,9,10,16,17-Hexakis(3-dietylaminophenoxy)-23(3-hydroxy-3-methyl-1-butynyl)- phthalocyaninato zinc(II) (**5**).* A dimethylaminoethanol (2 mL) solution of **3** (454 mg, 1 mmol), **4** (70 mg, 0.33 mmol), and $ZnCl_2$ (91 mg, 0.67 mmol) was stirred at reflux under nitrogen atmosphere for 12 h. The reaction was allowed to cool to room temperature, and the crude was precipitated in methanol/water mixture. The resulting green precipitate was collected by filtration and washed with water, then methanol. The product was dissolved with $CHCl_3$, then dried over Na_2SO_4. After it dried, the resulting crude product was purified by two consecutive column chromatographies on silica gel using first CH_2Cl_2/MeOH (50:1) and then CH_2Cl_2/MeOH (100:1) as eluents, affording **5** as a green solid in the second fraction.

Yield: 110 mg (%20); **^{1}H NMR** (500 MHz, $CDCl_3$ + one drop of d_5-pyridine, 25 °C), δ 9.39 (s, 1H), 9.29 (d, 1H), 9.12 (s, 1H), 9.07−9.04 (m, 5H), 8.10 (d, 1H), 7.26−7.19 (m, 6H), 6.68−6.50 (m, 18H), 3.35 (m, 24H), 1.79 (s, 6H), 1.21−1.17 (m, 36H) ppm. **^{13}C NMR** (126 MHz, $CDCl_3$ + one drop d_5-pyridine, 25 °C), δ 159.08, 159.07, 159.03, 158.94, 158.8, 153.94, 153.85, 153.81, 153.35, 153.27, 152.78, 158.75, 134.40, 134.26, 132.07, 130.19, 130.15, 130.06, 126.11, 123.55, 122.52, 114.39, 114.27, 113.97, 113.59, 109.99, 107.37, 107.28, 107.25, 107.23, 105.51, 105.14, 105.11, 105.03, 104.98, 102.90, 102.65, 102.54, 102.50, 102.44, 96.05, 82.82, 65.33, 44.47, 31.73, 12.66 ppm. **FT-IR** υ_{max} (cm^{-1}): 3296.70, 3069.81, 2966.62, 2925.74, 2870.32, 1603.88, 1567.70, 1487.77, 1446.40, 1394.42, 1356.10, 1262.98, 1195.85, 1172.36, 1133.98, 1089.72, 1030.93, 989.03, 962.29, 885.23, 831.03, 787.86, 745.36, 686.31. **UV/vis** (CH_2Cl_2): λ_{max}/nm = 686, 619, 354, 257. **MS** (MALDI-TOF), dithranol: m/z calcd: 1636.72; found: 1636.446 [M]$^+$.

*2,3,9,10,16,17-Hexakis(3-dietylaminophenoxy)-23etynylphthalocyaninato zinc(II) (**6**).* A dry toluene (2 mL) solution of phthalocyanine **5** (108 mg, 0.07 mmol) and dry NaOH (3 mg, 0.075 mmol) was stirred in a 10 mL flask under reflux in nitrogen atmosphere for 8 h. The solvent was removed at the rotary evaporator, and the solid residue was extracted with CH_2Cl_2 and washed with water. The organic phase was dried over Na_2SO_4. After evaporation of the solvent the resulting crude product was purified by chromatography on silica with CH_2Cl_2/methanol (50:1).

^{1}H NMR (500 MHz, $CDCl_3$ + 1 drop d_5-pyridine, 25 °C), δ 9.49 (s, 1H), 9.30−9.28 (d, 1H), 9.09 (s, H), 9.07 (s, H), 9.05−9.04 (m, 4H), 8.18−8.16 (d, 1H), 7.23−7.19 (m, 8H), 6.68−6.50 (m, 18H), 3.38−3.34 (m, 24H), 1.18−1.16 (m, 36H) ppm. **^{13}C NMR** (126 MHz, $CDCl_3$ + 1 drop d_5-pyridine, 25 °C), δ 159.09, 158.93, 158.79, 154.06, 153.97, 153.90, 153.32, 153.14, 152.38, 150.97, 150.93, 150.56, 150.16, 150.13, 149.59, 149.55, 138.07, 137.81, 134.71, 134.67, 134.56, 134.21, 132.41, 130.20, 130.16, 130.07, 126.70, 122.59, 122.44, 114.45, 114.40, 114.29, 113.60, 113.55, 107.46, 107.38, 107.28, 107.22, 105.52, 105.49, 105.11, 104.97, 102.94, 102.90, 102.53, 102.42, 84.61, 78.59, 65.83, 44.49, 12.66 ppm. **FT-IR** υ_{max} (cm^{-1}): 3279.12, 3063.73, 2969.24, 2923.07, 2865.93, 1607.23, 1569.62, 1497.70, 1449.67, 1401.94, 1356.74, 1275.71, 1199.94, 1135.91, 1091.40, 1032.26, 989.25, 962.29, 885.35, 831.85, 747.32, 686,75. **UV/vis** (CH_2Cl_2): λ_{max}/nm = 685, 620, 355, 258. **MS** (MALDI-TOF), dithranol: m/z calcd: 1578.68; found: 1578.659 [M]$^+$.

*2,3,9,10,16,17-Hexakis(3-dietylaminophenoxy)-23-etynylphenyl-(2-ferrocenyl-o-carborane)phthalocyaninato zinc(II) (**7**).* A dry toluene/TEA (2:1) mixture (15 mL) was subjected to deoxygenation with nitrogen and poured over a mixture of **6** (50 mg, 0.032 mmol), **2** (20.1 mg, 0.038 mmol), $Pd(PPh_3)_4$ (1.9 mg, 0.0016 mmol), and CuI (0.6 mg, 0.003 mmol). The mixture was stirred under nitrogen for 16 h at 80 °C. The product was purified by two consecutive column chromatographies on silica gel using first CH_2Cl_2/MeOH (30:1) and then CH_2Cl_2/MeOH (100:1) as eluents, affording **7** as a green solid.

Yield: 39 mg (62%); **^{1}H NMR** (500 MHz, $CDCl_3$ + one drop of d_5-pyridine, 25 °C), δ 9.50 (s, 1H), 9.33 (d, 1H), 9.12 (s, 1H), 9.08 (s,1H), 9.05−9.03 (m, 4H), 8.15 (d, 1H), 7.45−7.41 (m, 4H), 7.24−7.10 (m, 6H), 6.69−6.50 (m, 18H), 4.23 (t, 2H), 4.22 (s, 5H), 4.04 (t, 2H), 3.36 (m, 24H), 3.1−2(b, 10H), 1.21 (m, 36H) ppm. **^{13}C NMR** (126 MHz, $CDCl_3$ + one drop d_5-pyridine, 25 °C), δ 160.81, 159.06, 159.00, 158.98, 158.85, 158.79, 154.36, 153.81, 153.63, 153.54, 153.43, 153.26, 153.15, 153.10, 153.07, 150.70, 150.53, 150.40, 150.35, 150.20, 150.17, 149.61, 149.58, 149.55, 149.53, 140.45, 134.61, 134.50, 134.44, 134.43, 134.35, 134.32, 132.97, 130.14, 130.05, 124.01, 121.52, 119.61, 116.90, 114.31, 114.18, 114.13, 113.80, 113.73, 110.33, 107.48, 107.30, 107.21, 105.44, 105.42, 105.10, 105.08, 105.03, 102.80, 102.73, 102.50, 102.47, 102.46, 93.07, 89.72, 85.49, 84.97, 82.87, 71.22, 70.40, 68.79, 44.45, 12.67 ppm. **^{11}B NMR** (CDCl$_3$, 25 °C), δ −2.05, −9.89 ppm. **FT-IR** υ_{max} (cm^{-1}): 3076.92, 2969.93, 2936.26, 2870.32, 2575.82, 1609.90, 1569.96, 1498.65, 1403.14, 1275.92, 1200.98, 1135.26, 1091.32, 1033.13, 886.85, 749.34. **UV/vis** (CH_2Cl_2): λ_{max}/nm = 688, 621, 356, 260. **Elemental analysis** (%) calcd for $C_{112}H_{116}B_{10}FeN_{14}O_6Zn$: C 67.82, H 5.89, N 9.89; found: C 67.54, H 6.01, N 9.98.

CONCLUSION

Multifunctional materials offer great opportunities for the development of organic semiconducting devices. Existing aromatic systems, which have high π-electron delocalization, provide applications in the OFET technology. Here, we have reported the synthesis of an unsymmetrical phthalocyanine derivative functionalized with the ferrocenylcarborane moiety. The semiconducting performance of the compounds as an active layer in OFETs was investigated, which produces bottom-gate top-contact OFET devices using the transfer and output characteristics of the devices. This work has demonstrated the possibility of using an unsymmetrical phthalocyanine derivative functionalized with the ferrocenylcarborane moiety as an active layer in an OFET device with high hole mobility and high capacitance density. The overall evaluation of the results suggests that a thin film of **7** is a promising material for the fabrication of OFETs with high charge-carrier mobility and low operating voltage.

DOI: 10.1021/acs.inorgchem.7b03097
Inorg. Chem. XXXX, XXX, XXX−XXX

■ ASSOCIATED CONTENT

Supporting Information

The Supporting Information is available free of charge on the ACS Publications website at DOI: 10.1021/acs.inorgchem.7b03097.

MS, NMR, FT-IR, UV−vis spectra and crystallographic data (PDF)

Accession Codes

CCDC 1586894 contains the supplementary crystallographic data for this paper. These data can be obtained free of charge via www.ccdc.cam.ac.uk/data_request/cif, or by emailing data_request@ccdc.cam.ac.uk, or by contacting The Cambridge Crystallographic Data Centre, 12 Union Road, Cambridge CB2 1EZ, UK; fax: +44 1223 336033.

■ AUTHOR INFORMATION

Corresponding Author

*E-mail: esin@itu.edu.tr.

ORCID

Ilgın Nar: 0000-0003-2300-3071

Esin Hamuryudan: 0000-0002-1732-8585

Notes

The authors declare no competing financial interest.

■ ACKNOWLEDGMENTS

This work was supported by the Research Fund of the Istanbul Technical Univ.

■ REFERENCES

(1) (a) Choi, H. H.; Park, J.; Huh, S.; Lee, S. K.; Moon, B.; Han, S. W.; Hwang, C.; Cho, K. Photoelectric Memory Effect in Graphene Heterostructure Field-Effect Transistors Based on Dual Dielectrics. *ACS Photonics* **2017**, DOI: 10.1021/acsphotonics.7b01132. (b) Hu, B.-L.; Zhang, K.; An, C.; Pisula, W.; Baumgarten, M. Thiadiazoloquinoxaline-Fused Naphthalenediimides for n-Type Organic Field-Effect Transistors (OFETs). *Org. Lett.* **2017**, *19* (23), 6300−6303. (c) Singla, P.; Van Steerteghem, N.; Kaur, N.; Ashar, A. Z.; Kaur, P.; Clays, K.; Narayan, K. S.; Singh, K. Multifunctional geometrical isomers of ferrocene-benzo[1,2-b:4,5-b[prime or minute]]difuran-2,6-(3H,7H)-dione adducts: second-order nonlinear optical behaviour and charge transport in thin film OFET devices. *J. Mater. Chem. C* **2017**, *5* (3), 697−708. (d) Zhang, X.; Chi, Z.; Xu, B.; Jiang, L.; Zhou, X.; Zhang, Y.; Liu, S.; Xu, J. Multifunctional organic fluorescent materials derived from 9,10-distyrylanthracene with alkoxyl endgroups of various lengths. *Chem. Commun.* **2012**, *48* (88), 10895−10897.

(2) (a) Murphy, A. R.; Fréchet, J. M. J. Organic Semiconducting Oligomers for Use in Thin Film Transistors. *Chem. Rev.* **2007**, *107* (4), 1066−1096. (b) Mishra, A.; Ma, C.-Q.; Bäuerle, P. Functional Oligothiophenes: Molecular Design for Multidimensional Nanoarchitectures and Their Applications. *Chem. Rev.* **2009**, *109* (3), 1141−1276. (c) Xia, D.; Marszalek, T.; Li, M.; Guo, X.; Baumgarten, M.; Pisula, W.; Müllen, K. Solution-Processable n-Type Organic Semiconductors Based on Angular-Shaped 2-(12H-Dibenzofluoren-12-ylidene)malononitrilediimide. *Org. Lett.* **2015**, *17* (12), 3074−3077. (d) Anthony, J. E. Functionalized Acenes and Heteroacenes for Organic Electronics. *Chem. Rev.* **2006**, *106* (12), 5028−5048. (e) Ie, Y.; Ueta, M.; Nitani, M.; Tohnai, N.; Miyata, M.; Tada, H.; Aso, Y. Air-Stable n-Type Organic Field-Effect Transistors Based on 4,9-Dihydro-s-indaceno[1,2-b:5,6-b′]dithiazole-4,9-dione Unit. *Chem. Mater.* **2012**, *24* (16), 3285−3293. (f) Kim, J.; Rim, Y. S.; Liu, Y.; Serino, A. C.; Thomas, J. C.; Chen, H.; Yang, Y.; Weiss, P. S. Interface Control in Organic Electronics Using Mixed Monolayers of Carboranethiol Isomers. *Nano Lett.* **2014**, *14* (5), 2946−2951. (g) Nitani, M.; Ie, Y.; Tada, H.; Aso, Y. Solution-Processable n-Type Organic Field-Effect Transistor (OFET) Materials Based on Carbonyl-Bridged Bithiazole and Dioxocyclopentene-Annelated Thiophenes. *Chem. - Asian J.* **2011**, *6* (9), 2352−2361.

(3) Dimitrakopoulos, C. D.; Mascaro, D. J. Organic thin-film transistors: A review of recent advances. *IBM J. Res. Dev.* **2001**, *45* (1), 11−27.

(4) Nakanotani, H.; Adachi, C. In *Physics of Organic Semiconductors;* Wiley-VCH Verlag GmbH & Co. KGaA, 2012; pp 603−621.

(5) (a) Li, Z.; Li, X.; Li, J.; Hu, Y. *Youji Huaxue* **2013**, *33*, 891. (b) Kelley, T. W.; Baude, P. F.; Gerlach, C.; Ender, D. E.; Muyres, D.; Haase, M. A.; Vogel, D. E.; Theiss, S. D. Recent Progress in Organic Electronics: Materials, Devices, and Processes. *Chem. Mater.* **2004**, *16* (23), 4413−4422. (c) Koca, A.; Kasım Şener, M.; Koçak, M. B.; Gül, A. Investigation of the electrocatalytic activity of metalophthalocyanine complexes for hydrogen production from water. *Int. J. Hydrogen Energy* **2006**, *31* (15), 2211−2216. (d) Fernández-Ariza, J.; Krick Calderón, R. M.; Rodríguez-Morgade, M. S.; Guldi, D. M.; Torres, T. Phthalocyanine−Perylenediimide Cart Wheels. *J. Am. Chem. Soc.* **2016**, *138* (39), 12963−12974. (e) Ikeuchi, T.; Mori, S.; Kobayashi, N.; Kimura, M. Low-Symmetrical Zinc(II) Benzonaphthoporphyrazine Sensitizers for Light-Harvesting in Near-IR Region of Dye-Sensitized Solar Cells. *Inorg. Chem.* **2016**, *55* (10), 5014−5018.

(6) (a) Bora, M.; Schut, D.; Baldo, M. A. Combinatorial Detection of Volatile Organic Compounds Using Metal−Phthalocyanine Field Effect Transistors. *Anal. Chem.* **2007**, *79* (9), 3298−3303. (b) Tang, Q.; Li, H.; Liu, Y.; Hu, W. High-Performance Air-Stable n-Type Transistors with an Asymmetrical Device Configuration Based on Organic Single-Crystalline Submicrometer/Nanometer Ribbons. *J. Am. Chem. Soc.* **2006**, *128* (45), 14634−14639. (c) Locklin, J.; Shinbo, K.; Onishi, K.; Kaneko, F.; Bao, Z.; Advincula, R. C. Ambipolar Organic Thin Film Transistor-like Behavior of Cationic and Anionic Phthalocyanines Fabricated Using Layer-by-Layer Deposition from Aqueous Solution. *Chem. Mater.* **2003**, *15* (7), 1404−1412. (d) Duruk, E. G.; Yenilmez, H. Y.; Altindal, A.; Altuntas Bayir, Z. Microwave-assisted synthesis of novel non-peripherally substituted metallophthalocyanines and their sensing behaviour for a broad range of Lewis bases. *Dalton Trans.* **2015**, *44* (21), 10060−10068.

(7) (a) Chaidogiannos, G.; Petraki, F.; Glezos, N.; Kennou, S.; Nešpůrek, S. Soluble substituted phthalocyanines for OFET applications. *Mater. Sci. Eng., B* **2008**, *152* (1), 105−108. (b) Li, R.; Ma, P.; Dong, S.; Zhang, X.; Chen, Y.; Li, X.; Jiang, J. Synthesis, Characterization, and OFET Properties of Amphiphilic Heteroleptic Tris(phthalocyaninato) Europium(III) Complexes with Hydrophilic Poly(oxyethylene) Substituents. *Inorg. Chem.* **2007**, *46* (26), 11397−11404. (c) Gao, Y.; Ma, P.; Chen, Y.; Zhang, Y.; Bian, Y.; Li, X.; Jiang, J.; Ma, C. Design, Synthesis, Characterization, and OFET Properties of Amphiphilic Heteroleptic Tris(phthalocyaninato) Europium(III) Complexes. The Effect of Crown Ether Hydrophilic Substituents. *Inorg. Chem.* **2009**, *48* (1), 45−54. (d) Lu, G.; Kong, X.; Ma, P.; Wang, K.; Chen, Y.; Jiang, J. Amphiphilic (Phthalocyaninato) (Porphyrinato) Europium Triple-Decker Nanoribbons with Air-Stable Ambipolar OFET Performance. *ACS Appl. Mater. Interfaces* **2016**, *8* (9), 6174−6182.

(8) (a) Ozer, L. M.; Ozer, M.; Altindal, A.; Ozkaya, A. R.; Salih, B.; Bekaroglu, O. Synthesis, characterization, OFET and electrochemical properties of novel dimeric metallophthalocyanines. *Dalton Trans.* **2013**, *42* (18), 6633−6644. (b) Basak, A. S.; Ozkaya, A. R.; Altindal, A.; Salih, B.; Sengul, A.; Bekaroglu, O. Synthesis, characterization, oxygen electrocatalysis and OFET properties of novel mono- and ball-type metallophthalocyanines. *Dalton Trans.* **2014**, *43* (15), 5858−5870.

(9) (a) Poater, J.; Solà, M.; Viñas, C.; Teixidor, F. Hückel's Rule of Aromaticity Categorizes Aromatic closo Boron Hydride Clusters. *Chem. - Eur. J.* **2016**, *22* (22), 7437−7443. (b) Poater, J.; Solà, M.; Viñas, C.; Teixidor, F. π Aromaticity and Three-Dimensional Aromaticity: Two sides of the Same Coin? *Angew. Chem., Int. Ed.* **2014**, *53* (45), 12191−12195.

(10) (a) Spokoyny, A. M.; Machan, C. W.; Clingerman, D. J.; Rosen, M. S.; Wiester, M. J.; Kennedy, R. D.; Stern, C. L.; Sarjeant, A. A.;

DOI: 10.1021/acs.inorgchem.7b03097
Inorg. Chem. XXXX, XXX, XXX−XXX

Mirkin, C. A. A coordination chemistry dichotomy for icosahedral carborane-based ligands. *Nat. Chem.* **2011**, *3*, 590. (b) Grimes, R. N. In *Carboranes,* 3rd ed.; Academic Press: Boston, MA, 2016; pp 7−18. (c) Núñez, R.; Farràs, P.; Teixidor, F.; Viñas, C.; Sillanpää, R.; Kivekäs, R. A Discrete P···I I···P Assembly: The Large Influence of Weak Interactions on the 31P NMR Spectra of Phosphane−Diiodine Complexes. *Angew. Chem., Int. Ed.* **2006**, *45* (8), 1270−1272.

(11) Teixidor, F.; Barberà, G.; Vaca, A.; Kivekäs, R.; Sillanpää, R.; Oliva, J.; Viñas, C. Are Methyl Groups Electron-Donating or Electron-Withdrawing in Boron Clusters? Permethylation of o-Carborane. *J. Am. Chem. Soc.* **2005**, *127* (29), 10158−10159.

(12) Tsuboya, N.; Lamrani, M.; Hamasaki, R.; Ito, M.; Mitsuishi, M.; Miyashita, T.; Yamamoto, Y. Nonlinear optical properties of novel carborane-ferrocene conjugated dyads. Electron-withdrawing characteristics of carboranes. *J. Mater. Chem.* **2002**, *12* (9), 2701−2705.

(13) (a) Benhabbour, S. R.; Parrott, M. C.; Gratton, S. E. A.; Adronov, A. Synthesis and Properties of Carborane-Containing Dendronized Polymers. *Macromolecules* **2007**, *40* (16), 5678−5688. (b) González-Campo, A.; Ferrer-Ugalde, A.; Viñas, C.; Teixidor, F.; Sillanpää, R.; Rodríguez-Romero, J.; Santillan, R.; Farfán, N.; Núñez, R. A Versatile Methodology for the Controlled Synthesis of Photoluminescent High-Boron-Content Dendrimers. *Chem. - Eur. J.* **2013**, *19* (20), 6299−6312. (c) Cabrera-González, J.; Xochitiotzi-Flores, E.; Viñas, C.; Teixidor, F.; García-Ortega, H.; Farfán, N.; Santillan, R.; Parella, T.; Núñez, R. High-Boron-Content Porphyrin-Cored Aryl Ether Dendrimers: Controlled Synthesis, Characterization, and Photophysical Properties. *Inorg. Chem.* **2015**, *54* (10), 5021−5031.

(14) Marshall, J.; Hooton, J.; Han, Y.; Creamer, A.; Ashraf, R. S.; Porte, Y.; Anthopoulos, T. D.; Stavrinou, P. N.; McLachlan, M. A.; Bronstein, H.; Beavis, P.; Heeney, M. Polythiophenes with vinylene linked ortho, meta and para-carborane sidechains. *Polym. Chem.* **2014**, *5* (21), 6190−6199.

(15) (a) Cioran, A. M.; Musteti, A. D.; Teixidor, F.; Krpetić, Ž.; Prior, I. A.; He, Q.; Kiely, C. J.; Brust, M.; Viñas, C. Mercaptocarborane-Capped Gold Nanoparticles: Electron Pools and Ion Traps with Switchable Hydrophilicity. *J. Am. Chem. Soc.* **2012**, *134* (1), 212−221. (b) Grzelczak, M. P.; Danks, S. P.; Klipp, R. C.; Belic, D.; Zaulet, A.; Kunstmann-Olsen, C.; Bradley, D. F.; Tsukuda, T.; Viñas, C.; Teixidor, F.; Abramson, J. J.; Brust, M. Ion Transport across Biological Membranes by Carborane-Capped Gold Nanoparticles. *ACS Nano* **2017**, *11* (12), 12492−12499.

(16) Saha, A.; Oleshkevich, E.; Vinas, C.; Teixidor, F. Biomimetic Inspired Core−Canopy Quantum Dots: Ions Trapped in Voids Induce Kinetic Fluorescence Switching. *Adv. Mater.* **2017**, *29*, 1704238.

(17) (a) Cabrera-Gonzalez, J.; Ferrer-Ugalde, A.; Bhattacharyya, S.; Chaari, M.; Teixidor, F.; Gierschner, J.; Nunez, R. Fluorescent carborane-vinylstilbene functionalised octasilsesquioxanes: synthesis, structural, thermal and photophysical properties. *J. Mater. Chem. C* **2017**, *5*, 10211. (b) Ferrer-Ugalde, A.; González-Campo, A.; Viñas, C.; Rodríguez-Romero, J.; Santillan, R.; Farfán, N.; Sillanpää, R.; Sousa-Pedrares, A.; Núñez, R.; Teixidor, F. Fluorescence of New o-Carborane Compounds with Different Fluorophores: Can it be Tuned? *Chem. - Eur. J.* **2014**, *20* (32), 9940−9951. (c) Kim, S.-Y.; Cho, Y.-J.; Jin, G. F.; Han, W.-S.; Son, H.-J.; Cho, D. W.; Kang, S. O. Intriguing emission properties of triphenylamine-carborane systems. *Phys. Chem. Chem. Phys.* **2015**, *17* (24), 15679−15682. (d) Berksun, E.; Nar, I.; Atsay, A.; Ozcesmeci, I.; Gelir, A.; Hamuryudan, E. Synthesis and photophysical properties of porphyrin-BODIPY dyad and porphyrin-o-carborane-BODIPY triad. *Inorg. Chem. Front.* **2018**, *5*, 200. (e) Cabrera-Gonzalez, J.; Ferrer-Ugalde, A.; Bhattacharyya, S.; Chaari, M.; Teixidor, F.; Gierschner, J.; Nunez, R. Fluorescent carborane-vinylstilbene functionalised octasilsesquioxanes: synthesis, structural, thermal and photophysical properties. *J. Mater. Chem. C* **2017**, *5* (39), 10211−10219.

(18) (a) Eo, M.; Bae, H. J.; Hong, M.; Do, Y.; Cho, S.; Lee, M. H. Synthesis and electron transporting properties of methanofullerene-o-carborane dyads in organic field-effect transistors. *Dalton Trans.* **2013**, *42* (22), 8104−8112. (b) Núñez, R.; Tarrés, M.; Ferrer-Ugalde, A.; de Biani, F. F.; Teixidor, F. Electrochemistry and Photoluminescence of Icosahedral Carboranes, Boranes, Metallacarboranes, and Their Derivatives. *Chem. Rev.* **2016**, *116* (23), 14307−14378.

(19) Misra, R.; Maragani, R.; Jadhav, T.; Mobin, S. M. Ferrocenyl end capped molecular rods: synthesis, structure, and properties. *New J. Chem.* **2014**, *38* (4), 1446−1457.

(20) (a) Özçeşmeci, M.; Hamuryudan, E. The synthesis and characterization of functionalized polyfluorinated phthalocyanines. *Dyes Pigm.* **2008**, *77* (2), 457−461. (b) Arslanoğlu, Y.; Hamuryudan, E. Synthesis and derivatization of near-IR absorbing titanylphthalocyanines with dimethylaminoethylsulfanyl substituents. *Dyes Pigm.* **2007**, *75* (1), 150−155.

(21) (a) Dei, D.; Chiti, G.; De Filippis, M. P.; Fantetti, L.; Giuliani, F.; Giuntini, F.; Soncin, M.; Jori, G.; Roncucci, G. Phthalocyanines as photodynamic agents for the inactivation of microbial pathogens. *J. Porphyrins Phthalocyanines* **2006**, *10* (03), 147−159. (b) Karaoğlu, H. R. P.; Koca, A.; Koçak, M. B. Synthesis, electrochemical and spectroelectrochemical characterization of novel soluble phthalocyanines bearing chloro and quaternizable bulky substituents on peripheral positions. *Dyes Pigm.* **2012**, *92* (3), 1005−1017.

(22) Maya, E. M.; Haisch, P.; Vázquez, P.; Torres, T. Synthesis and characterization of tetraethynylphthalocyanines. *Tetrahedron* **1998**, *54* (17), 4397−4404.

(23) (a) Garcia-Iglesias, M.; Torres, T.; Gonzalez-Rodriguez, D. Well-defined, persistent, chiral phthalocyanine nanoclusters via G-quadruplex assembly. *Chem. Commun.* **2016**, *52* (60), 9446−9449. (b) Ik Yang, S.; Li, J.; Sun Cho, H.; Kim, D.; Bocian, D. F.; Holten, D.; Lindsey, J. S. Synthesis and excited-state photodynamics of phenylethyne-linked porphyrin-phthalocyanine dyads. *J. Mater. Chem.* **2000**, *10* (2), 283−296. (c) García-Frutos, E. M.; Fernández-Lázaro, F.; Maya, E. M.; Vázquez, P.; Torres, T. Copper-Mediated Synthesis of Phthalocyanino-Fused Dehydro[12]- and [18]annulenes. *J. Org. Chem.* **2000**, *65* (21), 6841−6846.

(24) Korotvička, A.; Šnajdr, I.; Štěpnička, P.; Císařová, I.; Janoušek, Z.; Kotora, M. Synthesis, Molecular Structure, and Electrochemistry of 1-Ferrocenyl-1,2-dicarba-closo-dodecaboranes. *Eur. J. Inorg. Chem.* **2013**, *2013* (15), 2789−2798.

(25) Oliva, J. M.; Allan, N. L.; Schleyer, P. v. R.; Viñas, C.; Teixidor, F. Strikingly Long C···C Distances in 1,2-Disubstituted ortho-Carboranes and Their Dianions. *J. Am. Chem. Soc.* **2005**, *127* (39), 13538−13547.

(26) (a) Akkurt, B.; Hamuryudan, E. Enhancement of solubility via esterification: Synthesis and characterization of octakis (ester)-substituted phthalocyanines. *Dyes Pigm.* **2008**, *79* (2), 153−158. (b) González-Cabello, A.; Vázquez, P.; Torres, T. A new phthalocyanine−ferrocene conjugated dyad. *J. Organomet. Chem.* **2001**, *637*, 751−756.

(27) Cabrera-González, J.; Sánchez-Arderiu, V.; Viñas, C.; Parella, T.; Teixidor, F.; Núñez, R. Redox-Active Metallacarborane-Decorated Octasilsesquioxanes. Electrochemical and Thermal Properties. *Inorg. Chem.* **2016**, *55* (22), 11630−11634.

(28) Mack, J.; Stillman, M. J. In *The Porphyrin Handbook;* Smith, K. M., Guilard, R., Eds.; Academic Press: Amsterdam, The Netherlands, 2003; pp 43−116.

(29) (a) L'Her, M.; Pondaven, A. In *The Porphyrin Handbook*; Smith, K. M., Guilard, R., Eds.; Academic Press: Amsterdam, The Netherlands, 2003; pp 117−169. (b) Follana-Berná, J.; Inan, D.; Blas-Ferrando, V. M.; Gorczak, N.; Ortiz, J.; Manjón, F.; Fernández-Lázaro, F.; Grozema, F. C.; Sastre-Santos, Á. Synthesis and Photophysical Properties of Conjugated and Nonconjugated Phthalocyanine−Perylenediimide Systems. *J. Phys. Chem. C* **2016**, *120* (46), 26508−26513.

(30) (a) Aydemir, M.; Karaoğlu, H. R. P.; Koçak, M. B.; Koca, A. Electropolymerization of Octakis Diethlyamino Substituted Metallophthalocyanines and Their Electrochromic Characterization. *J. Electrochem. Soc.* **2015**, *162* (3), H170−H178. (b) Karaoğlu, H. R. P.; Koca, A.; Koçak, M. B. The synthesis and electrochemistry of novel, symmetrical, octasubstituted phthalocyanines. *Synth. Met.* **2013**, *182*, 1−8.

DOI: 10.1021/acs.inorgchem.7b03097
Inorg. Chem. XXXX, XXX, XXX−XXX

(31) (a) Sze, S. M.; Ng, K. K. In *Physics of Semiconductor Devices;* John Wiley & Sons, Inc., 2006. (b) Singh, T. B.; Sariciftci, N. S. Progress in plastic electronic devices. *Annu. Rev. Mater. Res.* **2006**, *36* (1), 199−230.
(32) Brown, A. R.; Jarrett, C. P.; de Leeuw, D. M.; Matters, M. Field-effect transistors made from solution-processed organic semiconductors. *Synth. Met.* **1997**, *88* (1), 37−55.
(33) (a) Hong, F.; Guo, X.; Zhang, H.; Wei, B.; Zhang, J.; Wang, J. Preparation of highly oriented copper phthalocyanine film by molecular templating effects for organic field-effect transistor. *Org. Electron.* **2009**, *10* (6), 1097−1101. (b) Kraus, M.; Haug, S.; Brütting, W.; Opitz, A. Achievement of balanced electron and hole mobility in copper-phthalocyanine field-effect transistors by using a crystalline aliphatic passivation layer. *Org. Electron.* **2011**, *12* (5), 731−735.
(34) (a) Sirringhaus, H.; Brown, P. J.; Friend, R. H.; Nielsen, M. M.; Bechgaard, K.; Langeveld-Voss, B. M. W.; Spiering, A. J. H.; Janssen, R. A. J.; Meijer, E. W.; Herwig, P.; de Leeuw, D. M. Two-dimensional charge transport in self-organized, high-mobility conjugated polymers. *Nature* **1999**, *401*, 685. (b) Fox, M. A.; Nervi, C.; Crivello, A.; Batsanov, A. S.; Howard, J. A. K.; Wade, K.; Low, P. J. Structural, spectroscopic, electrochemical and computational studies of C,C′-diaryl-ortho-carboranes, 1-(4-XC6H4)-2-Ph-1,2-C2B10H10 (X = H, F, OMe, NMe2, NH2, OH and O−). *J. Solid State Electrochem.* **2009**, *13* (10), 1483−1495. (c) Hosoi, K.; Inagi, S.; Kubo, T.; Fuchigami, T. o-Carborane as an electron-transfer mediator in electrocatalytic reduction. *Chem. Commun.* **2011**, *47* (30), 8632−8634.
(35) Sheldrick, G. A short history of SHELX. *Acta Crystallogr., Sect. A: Found. Crystallogr.* **2008**, *64* (1), 112−122.
(36) Macrae, C. F.; Edgington, P. R.; McCabe, P.; Pidcock, E.; Shields, G. P.; Taylor, R.; Towler, M.; van de Streek, J. Mercury: visualization and analysis of crystal structures. *J. Appl. Crystallogr.* **2006**, *39* (3), 453−457.
(37) Sun, Y.; Liu, Y.; Wang, Y.; Di, C.; Wu, W.; Yu, G. Polymer gate dielectrics with self-assembled monolayers for high-mobility organic thin-film transistors based on copper phthalocyanine. *Appl. Phys. A: Mater. Sci. Process.* **2009**, *95* (3), 777−780.

DOI: 10.1021/acs.inorgchem.7b03097
Inorg. Chem. XXXX, XXX, XXX−XXX